Microporous and Mesoporous Materials

Porous and ultrahigh surface area SiOC ceramics based on perhydropolysilazane and polysiloxane --Manuscript Draft--

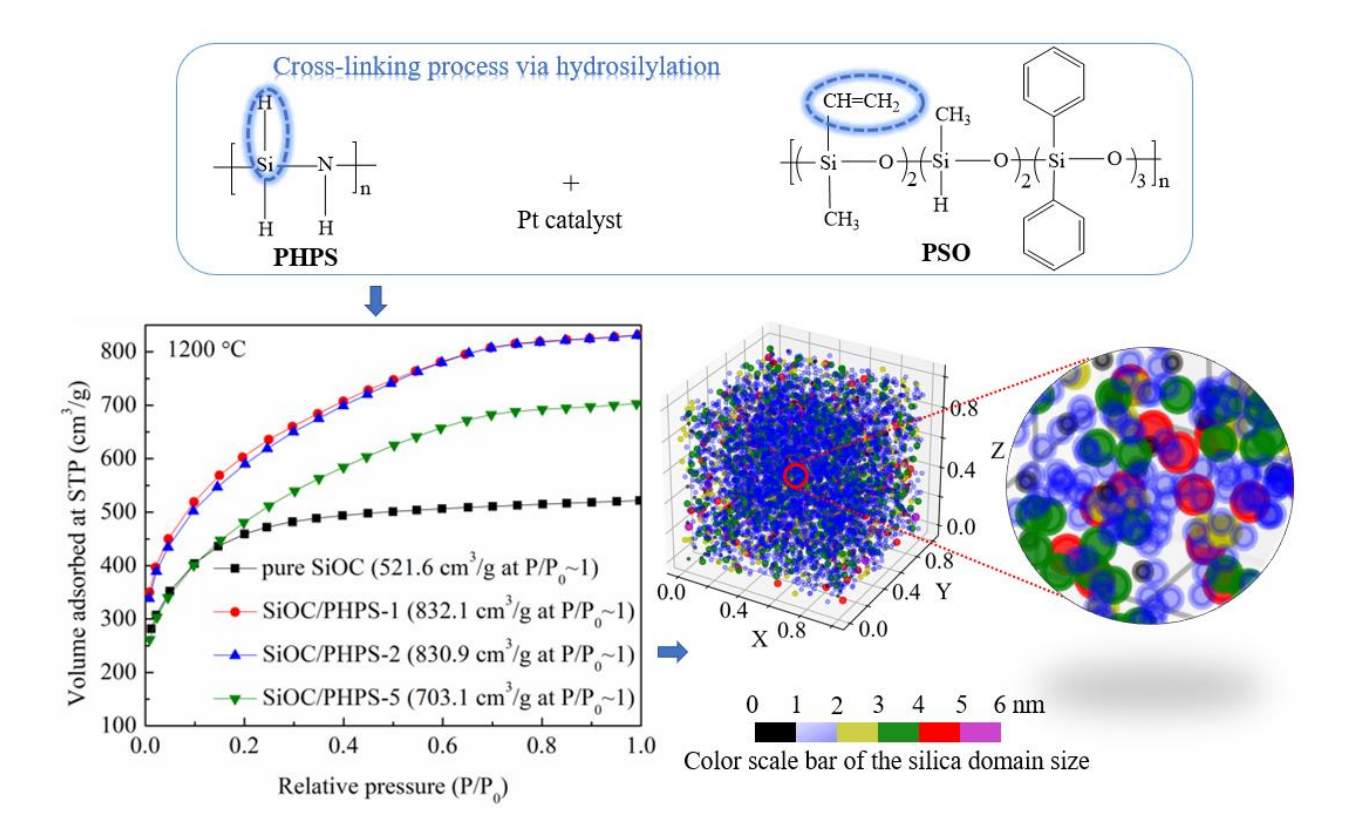
| Manuscript Number: | MICMAT-D-20-00471R1 |
|-----------------------|--|
| Article Type: | Full length article |
| Keywords: | polymer-derived ceramic; silicon oxycarbide; Perhydropolysilazane; pore; Specific surface area |
| Corresponding Author: | Kathy Lu, PhD Virginia Tech Blacksburg, VA United States |
| First Author: | Ni Yang |
| Order of Authors: | Ni Yang |
| | Kathy Lu, PhD |
| Abstract: | Micro-/meso-porous ceramics with ultrahigh surface areas are highly desired in high-temperature applications. In this work, formation of porous silicon oxycarbide (SiOC) is studied based on perhydropolysilazane (PHPS) and polysiloxane (PSO) precursors. The PHPS can be chemically anchored to the PSO by hydrosilylation reaction, due to the extensive Si-H bonds from the PHPS. The presence of water vapor during pyrolysis not only accelerates the hydrolysis of the PHPS additive, but also facilitates the Si-O-Si bond formation within the SiOC. The resulting SiOC material has the highest specific surface area (SSA) of ~2000 m 2 /g with an average pore size of 1.72nm. The effects of the PHPS additive on the phase evolution and the resulting porous SiOC after hydrogen fluoride (HF) etching are investigated. 3D view of pore distributions qualitatively illustrates the PHPS effect on the SiO 2 nanocluster formation in the SiOC. The difference between the experimental and calculated SSAs is explained based on the etchability and wall thickness of the SiO 2 domains. |

Highlights (for review)

Highlights

- PHPS can be anchored to PSO and facilitate the Si-O-Si bond formation in SiOC.
- Effects of PHPS addition on phase evolution of porous SiOC are investigated.
- An ultrahigh surface area of $\sim 2000 \text{ m}^2/\text{g}$ and a pore size of 1.72 nm are achieved.
- A model is used to calculate domain wall thickness and pore distribution in SiOC.

Graphical Abstract



<u>*</u>

Manuscript

Click here to view linked References

Porous and ultrahigh surface area SiOC ceramics based on perhydropolysilazane

and polysiloxane

Ni Yang, Kathy Lu*

Department of Materials Science and Engineering, Virginia Polytechnic Institute and State

University, Blacksburg, Virginia, 24061, USA

*Corresponding author: Email: klu@vt.edu

Declarations of interest: none

Abstract

Micro-/meso-porous ceramics with ultrahigh surface areas are highly desired in high-

temperature applications. In this work, formation of porous silicon oxycarbide (SiOC) is studied

based on perhydropolysilazane (PHPS) and polysiloxane (PSO) precursors. The PHPS can be

chemically anchored to the PSO by hydrosilylation reaction, due to the extensive Si-H bonds from

the PHPS. The presence of water vapor during pyrolysis not only accelerates the hydrolysis of the

PHPS additive, but also facilitates the Si-O-Si bond formation within the SiOC. The resulting SiOC

material has the highest specific surface area (SSA) of ~2000 m²/g with an average pore size of

1.72 nm. The effects of the PHPS additive on the phase evolution and the resulting porous SiOC

after hydrogen fluoride (HF) etching are investigated. 3D view of pore distributions qualitatively

illustrates the PHPS effect on the SiO₂ nanocluster formation in the SiOC. The difference between

the experimental and calculated SSAs is explained based on the etchability and wall thickness of

1

the SiO₂ domains.

Keywords:

Polymer-derived ceramic; Silicon oxycarbide; Perhydropolysilazane; Pore; Specific surface area

Introduction

Porous and high surface area ceramic materials are widely used as chemical reactors, sensors, electrodes, filters, catalyst supports, lightweight structure materials, molecular sieves, among others. The use of porous ceramics offers several excellent characteristics over other classes of porous materials [1]: good chemical stability, great specific strength and rigidity, and high thermal stability. In addition, the pore sizes and shapes of ceramics do not easily change under different stress loading conditions [2]. Proper choice of material species and techniques can make porous ceramics suitable for various harsh environments, such as under corrosive or high-temperature conditions.

In the last twenty years, preceramic polymers have been proven useful in preparation of high-temperature materials with tailored nanostructures and complex shapes [3-5]. Due to the need for high-temperature stable and oxidation-resistant applications, much attention has been paid to silicon oxycarbide (SiOC) [6-8], in which divalent oxygen atoms are partially replaced by tetravalent carbon atoms, thus enhancing thermal properties [9]. SiOC-related materials have been extensively investigated due to its wide use in semiconductor industry, coatings, medical devices, and so on [10-12]. Porous SiOC materials are an interesting system that can be prepared from pyrolysis of various polysiloxane (PSO) precursors under different processing conditions. A wide

range of unique SiOC microstructures can be adjusted to provide porous systems with a high surface area as well as thermal stability [13, 14].

Various fabrication processes [15-18], such as partial sintering, sacrificial fugitives, replica templates, and direct foaming, can create SiOC systems with a wide range of pore sizes. However, such processes can only produce macro pores [19]; and creating ultrahigh surface area SiOCs remains a great challenge. To generate mesopores, and more desirably micropores, only controlled phase separation at the molecular level is a viable method, which can lead to pore sizes with less than 10 nm along with narrow distributions.

There have been efforts to control phase separation of polymer precursors during crosslinking. Mixing of preceramic precursors with different architectures is a developed route for one-step fabrication [17, 20-22]. When a silicone resin is crosslinked with a conventional PSO, a dense polymeric green body is formed before creating porosity by gas evolution during pyrolysis. However, the number and size of the SiO₂ nanodomains (and thus pores) in the SiOC are closely related to the preceramic precursors and processing conditions [23]. The specific surface area decreases with increasing temperature due to the sintering of transient pores. The pyrolysis temperature can also significantly influence the phase separation and separated domain sizes. At low pyrolysis temperatures (800–1100 °C), the SiOC glasses only consist of a homogeneous network of mixed Si-O-C tetrahedral and free carbon species, which can be described as a SiC_xO_y matrix within the free carbon dispersed. At >1100 °C, amorphous SiO₂ nanodomains form. The mixed Si-O-C bonds between the SiO₂ nanodomains and graphitic layers are populated by SiO₁C₃, SiO₂C₂, and SiO₃C₁ tetrahedra with different ratios. After pyrolysis, SiO₂ nanodomains can be selectively etched away by hydrofluoric acid (HF), leaving behind nano-sized pores inside the SiOC matrix to create an ultrahigh surface area.

In our work [21, 23, 24], it is noted that the presence of water vapor during pyrolysis (500-700 °C) preferentially removes the free carbon in the SiOC matrix. SiC formation is suppressed due to the less dominant presence of carbon, along with some SiO₂ being reduced to Si. Water vapor accelerates the crystallization of the SiO₂ nanodomains. After the pyrolysis, these crystallized SiO₂ nanodomains can be selectively etched away with a HF solution to form a highly porous SiOC material. Tetraethyl orthosilicate (TEOS) [23] can be used as a SiO₂-forming additive to further react with an Ar + H₂O pyrolysis atmosphere. SiO₂ domains form from the hydrolysis and condensation of the TEOS with the water vapor, as well as from the phase separation of the SiOC matrix. After the removal of the SiO₂ domains from the HF etching, the specific surface area of the SiOC matrix increases from 1108.5 m²/g for the base PSO to 1953.9 m²/g for the PSO with TEOS.

Perhydropolysilazane (PHPS), an inorganic polymer composed only of Si-N, Si-H and N-H bonds [25], has been drawing more attention. PHPS can be converted to a SiO_x phase by two entirely different routes, either by reaction with water vapor or by a photolytic process with oxygen atoms [26]. In the presence of water vapor during pyrolysis, an oxidative process may occur. The hydrolysis of the massive Si-N and Si-H bonds results in the release of ammonia and hydrogen gas as well as the formation of silanol groups, before transforming into a SiO_x network in a subsequent thermally triggered condensation process. Interestingly, PHPS can be chemically attached to the PSO by hydrosilylation reaction and is potentially a desirable additive due to its cross-linking via platinum catalyzed hydrosilylation.

In this work, micro-/meso-porous SiOC ceramics are prepared through the addition of PHPS to a PSO precursor and pyrolyzed at 1100–1300 °C in an Ar + H₂O atmosphere. The SiO₂ domains can be etched away using HF to obtain high surface area SiOC bulk ceramics. The effects of the

PHPS content and pyrolysis temperature on the resulting phase evolution, specific surface area, pore volume, and average pore size of the SiOC ceramics are investigated.

2. Experimental part

A polysiloxane (PSO) SPR-684, a member of the Polyramic® family (Starfire Systems, Inc. Schenectady, NY), was used as the polymeric precursor. A commercially available perhydropolysilazane (PHPS NN 120- 20) solution in the form of 20 wt% PHPS in dibutyl ether (Clariant Advanced Materials, Sulzbach am Taunus, Germany) was used as an additive to the PSO precursor. A 2.1–2.4% platinum-divinyltetramethyldisiloxane complex in xylene (Pt catalyst, Gelest Inc. Morrisville, PA) was used as a catalyst.

First, four kinds of PHPS-containing PSO materials (Table 1) containing the Pt catalyst (1 wt% relative to PSO) were prepared by mixing a solution of PSO and PHPS (the molar ratio of Si in PSO: PHPS was 100:0, 100:1, 100:2, and 100:5, respectively) with magnetic stirring at 80 °C overnight in a glove box (Labstar^{pro}, MBRAUN[®]) until a homogeneous mixture formed. Before being poured into aluminum foil molds, the mixtures were vacuumed for 10 min at 1500 mTorr to remove bubbles inside the solutions. A blank group without any PHPS was prepared under the same conditions. The curing of the samples was performed in an oven at 100 °C for 12 hours, and then at 150 °C for 12 hours. The sample nomenclatures were given in Table 1.

Before pyrolysis, the crosslinked specimens (circular pieces within 10 mm of diameter and 2 mm of thickness) were placed into a zirconia crucible, covered with graphite mats, and put into a tube furnace (1730-20 Horizontal Tube Furnace, CM Furnaces Inc. Bloomfield, NJ). With a compressed argon (Industrial grade, AirGas, Inc., Radnor, PA) flow rate at 500 std cm³/min, the samples were pyrolyzed to 1100 °C, 1200 °C, or 1300 °C at a rate of 2 °C/min with a dwelling time

of 2 h at the peak temperature, before cooling to room temperature at a rate of 2 °C/min. During heating from 500°C to 700 °C, the Ar gas was bubbled through water at 60 °C, giving a gas flow with an Ar:H₂O molar ratio of approximately 5:1 [24]. Etching of the pyrolyzed samples was carried out in a HF solution (20 wt% HF in water) for 72 h. After that, all the samples were rinsed with deionized water three times and vacuum dried at 120 °C.

Table 1. Prepared samples and pyrolysis temperatures.

| | Mole ratio of Si atoms in | Pyrolysis | |
|-------------|---------------------------|------------------|--|
| Sample | PSO: PHPS | temperature (°C) | |
| Pure SiOC | 100:0 | 1100/1200/1300 | |
| SiOC/PHPS-1 | 100:1 | 1100/1200/1300 | |
| SiOC/PHPS-2 | 100:2 | 1100/1200/1300 | |
| SiOC/PHPS-5 | 100:5 | 1100/1200/1300 | |
| | | | |

Phase compositions of the pyrolyzed samples were investigated by using an X'Pert PRO diffractometer (PANalytical B.V.). The chemical bonding of the pyrolyzed samples was evaluated using Fourier Transform Infrared Spectroscopy (FT-IR) (Nicolet 8700 with Pike GladiATR attachment, Thermo Scientific, Waltham, MA) between 500 and 4000 cm⁻¹ wavenumber (4 cm⁻¹ resolutions, 128 scans). The specific surface area, pore size distribution, and specific pore volume of the etched samples were evaluated using nitrogen adsorption at 77 K with a Quantachrome Autosorb-1 (Quantachrome Instruments, Boynton Beach, FL). The samples were degassed up to 10^{-3} relative pressure (P/P_o) for 12 h at 300 °C before testing. The specific surface areas were

obtained by applying the Non-Local Density Functional Theory (NLDFT) theory to the N₂ adsorption results. The pore size distribution and specific pore volume were also derived by applying the NLDFT model and assuming cylindrical pores to the adsorption branch of the data. The densities of the etched samples were measured in triplicate by a pycnometer (AccuPyc II 1340, Micromeritics®, Norcross, GA) using He gas at an outlet pressure of 1.34 bars in a 7.8 cm³ sample cell. The 3D plots for the distribution of the SiO₂ domains were conducted using Spyder (Python 3.7).

3. Results and discussion

3. 1. Polymer to ceramic conversion

As shown in Fig. 1(a), PHPS consists of Si-H groups as well as silicon and nitrogen atoms alternating to form the basic backbone with all hydrogen substituents. For the PSO in Fig. 1(b), the crosslinking can be realized via a hydrosilylation catalyst, typically platinum complexes. It occurs between Si-H and –CH=CH₂ groups. The interactions between the PSO and PHPS species are illustrated in Fig. 1(c). Different from the physical mixing of additives and polymeric precursors [13], PHPS can be crosslinked with PSO by the hydrosilylation reaction of the Si-H bonds and the vinyl groups in the PSO [27], which has been confirmed by the disappearance of Si-H bonds in the PHPS precursors after crosslinking with PSO. No broad Si-H peaks at 800 - 950, and 2080 - 2280 cm⁻¹ [28] are observed in the FT-IR spectra of the crosslinked PSO-PHPS polymers (supplement Fig. S1). It is a fast reaction even at low temperatures (e.g., ~110 °C) [29]. Thus, PHPS can be chemically anchored to the network of the PSO without any physical segregation. Fig. 1(d) indicates a structure change in the PHPS involving the reaction of – NH—with water vapor during pyrolysis [30], which can result in extensive SiO₂ formation.

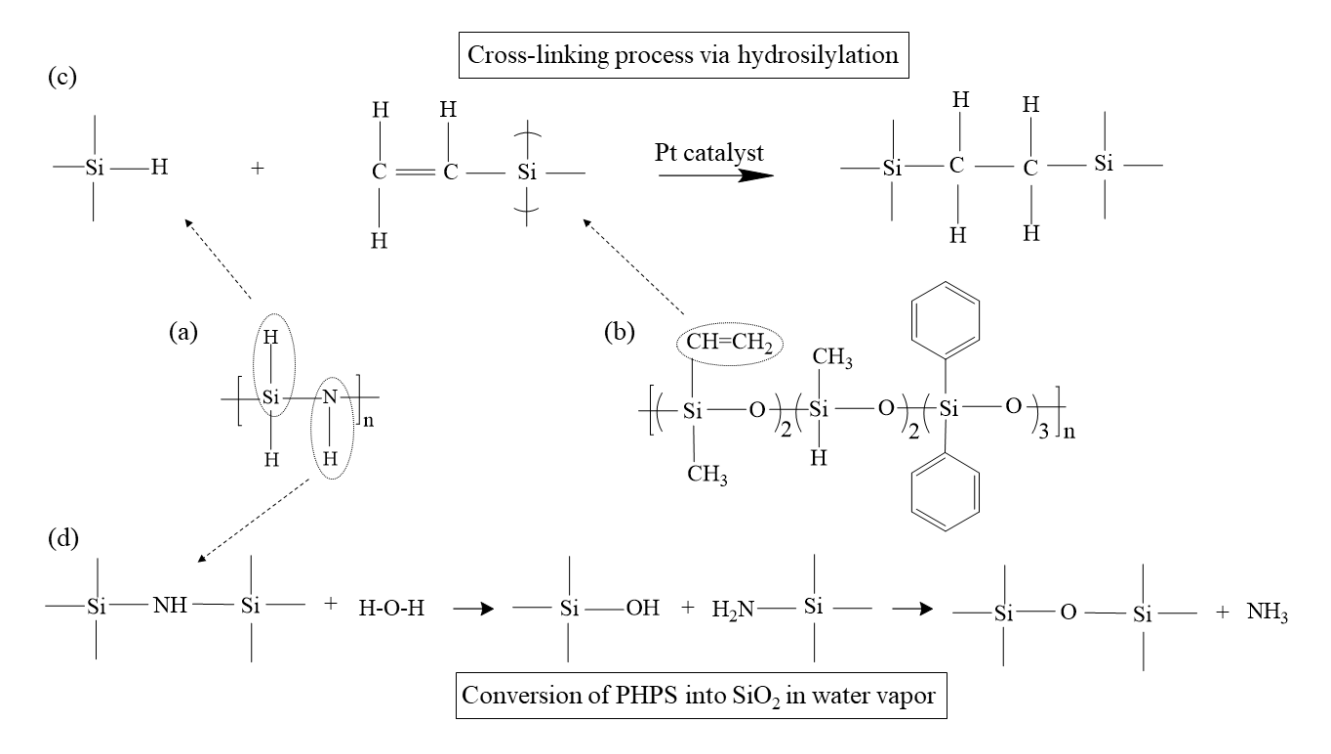


Fig. 1. Molecular structure of (a) perhydropolysilazane (PHPS), (b) polysiloxane (PSO) SPR-684, (c) cross-linking via platinum-catalyzed hydrosilylation, and (d) the conversion of the PHPS into SiO2 during pyrolysis.

The pyrolysis of the cured PSO-PHPS system involves the generation and escape of NH₃, CH₄, H₂, CO, CO₂, C₂H₆, and C₂H₄ gases, as well as various redistribution reactions among the Si-C, Si-H, and Si-O bonds. In the presence of water vapor during the pyrolysis period, the polymer to ceramic transformation occurs as follows [23, 31]:

$$Si-H + O-O \rightarrow Si-OH \tag{1}$$

$$Si-H + H-O-H \rightarrow Si-OH + H_2 \uparrow$$
 (2)

$$Si-CH_3 + H-O-H \rightarrow Si-OH + CH_4 \uparrow$$
 (3)

$$Si-CH2-Si + H-O-H \rightarrow Si-OH + Si-CH3$$
 (4)

$$Si-CH_3 + O-O \rightarrow Si-O-Si + H-O-H + CO \uparrow + CO_2 \uparrow$$
 (5)

$$Si-CH_2-CH_2-Si+H-O-H \rightarrow Si-OH+C_2H_6 \uparrow$$
 (6)

$$Si-CH=CH_2 + H-O-H \rightarrow Si-OH + C_2H_4 \uparrow \tag{7}$$

$$Si-C_6H_5 + H-O-H \rightarrow Si-OH + C_6H_6 \uparrow \tag{8}$$

$$\equiv Si-NH + H-O-H \rightarrow (\equiv Si-OH + \equiv Si-NH_2) \rightarrow \equiv Si-O-Si \equiv + NH_3 \uparrow \qquad (9)$$

The oxidation and hydrolysis of the Si–H groups from PHPS in the crosslinked samples can lead to extensive Si-OH groups as shown in the above equations (1-9). Hydrogen and nitrogen are gradually released from the system, and nitrogen can be almost completely eliminated at 600 °C as reported [32]. Water vapor accelerates not only the hydrolysis of PHPS, but also the Si-O-Si bond formation from the PSO-derived SiOC matrix. The plethora of the Si-OH groups can subsequently condense to generate extensive Si-O-Si bonds to form SiO₂-rich regions (Fig. 1(d)). Our previous study [24] also shows that water vapor preferentially removes the free carbon in the SiOC according to:

$$C_{free} + H_2O \rightarrow H_2\uparrow + CO\uparrow$$
 (10)

As a result, the SiOC phase and residual free carbon form. With the less dominant presence of free carbon, SiC and crystalline carbon formation is suppressed. More importantly, water vapor promotes the crystallization of the SiO₂ nanodomains. The amount and size of the SiO₂ nanodomains can be adjusted by controlling the dwelling time and amount of the water vapor during the polymer-to-ceramic conversion process.

In Fig. 2, the ceramic yields of the SiOC samples are displayed as a function of the PHPS content at 1100, 1200, and 1300 °C pyrolysis temperatures. For the pure SiOC ceramic, the pyrolysis temperature causes no significant change in the ceramic yield from 1100 °C to 1200 °C. From 1200 °C to 1300 °C, the ceramic yield decreases from 64.9 % to 60.9 % due to carbothermal reduction [21]:

$$SiO_2$$
 (amorphous) + C \rightarrow SiC (β) + CO \uparrow (11)

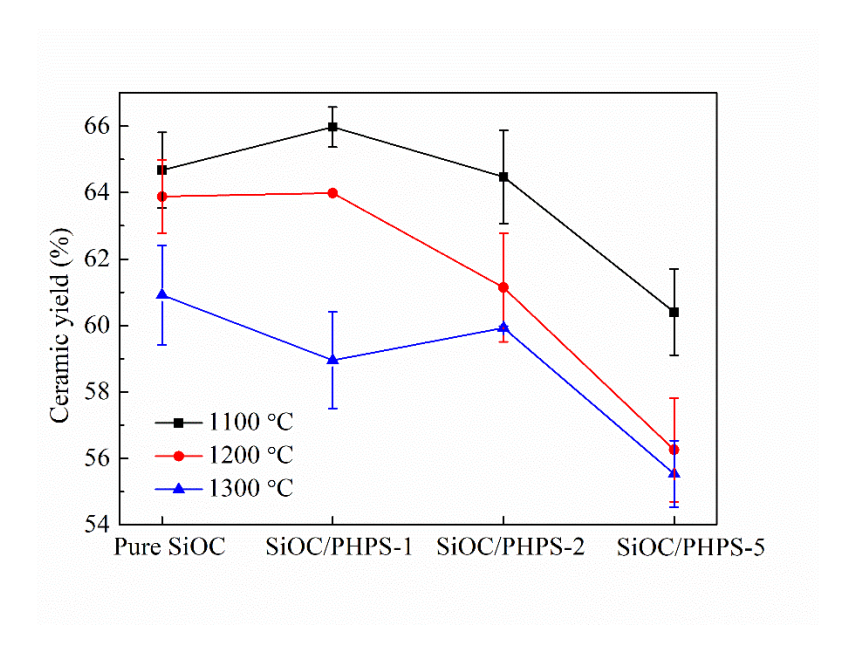


Fig. 2. Ceramic yield of different SiOC/PHPS samples pyrolyzed at 1100, 1200, and 1300 °C.

It is reasonable that higher pyrolysis temperature leads to lower ceramic yield. In general, higher percentage of PHPS addition also leads to lower ceramic yield regardless of the pyrolysis temperature. This decrease can be attributed to the hydrolysis and condensation of the Si-OH groups during the water vapor injection period, as well as the evaporation of gas species (CO, CO₂, etc.) [24] through equations (2-8). From 1100 °C to 1300 °C, the ceramic yield of SiOC/PHPS-1 decreases from 66.0 % to 60.0 %. The same trend also happens for SiOC/PHPS-2 (64.5 % to 60.0 %) and SiOC/PHPS-5 (60.4 % to 55.5 %). However, the mass loss in these systems is small, suggesting that the formation of SiC is limited due to the removal of the free C using water vapor in the early stage of the pyrolysis.

The volume shrinkage of all the SiOC samples pyrolyzed at 1100-1300 °C is shown in Table S1, in the range of 20.46%- 26.76%. Similar to our previous study [13], the shrinkage gradually decreases with an increasing filler content at a given pyrolysis temperature. It also means

that the filler can decrease thermal stress during the pyrolysis, prevent cracking, and facilitate intact sample formation.

3. 2. Phase evolution

Fig. 3 shows the FTIR spectra of the pure SiOC as well as SiOC/PHPS-1, SiOC/PHPS-2, and SiOC/PHPS-5 samples before the HF etching, pyrolyzed at 1200 °C. The chemical bonds in the spectra reflect the effect of the PHPS addition on the SiO₂ formation. All the pyrolyzed samples show broad peaks, except for the sharp peaks from SiOC/PHPS-5. For the pure SiOC, SiOC/PHPS-1 and SiOC/PHPS-2, two broad peaks between 1000-1100 cm⁻¹ and 750-850 cm⁻¹ can be assigned to the vibrational bonds of Si-O [23, 33]. With further chemical addition of PHPS into the SiOC system, the peaks become sharper and are located at 804 and 1098 cm⁻¹ due to the increasing amount of Si-O-Si bonds. This means that the addition of PHPS does facilitate the Si-O-Si formation in the SiOC matrix, and the amount of SiO₂ within the pyrolyzed samples increases from SiOC/PHPS-1 to SiOC/PHPS-5, consistent with the mass loss changes during the HF etching (shown in Fig. 5).

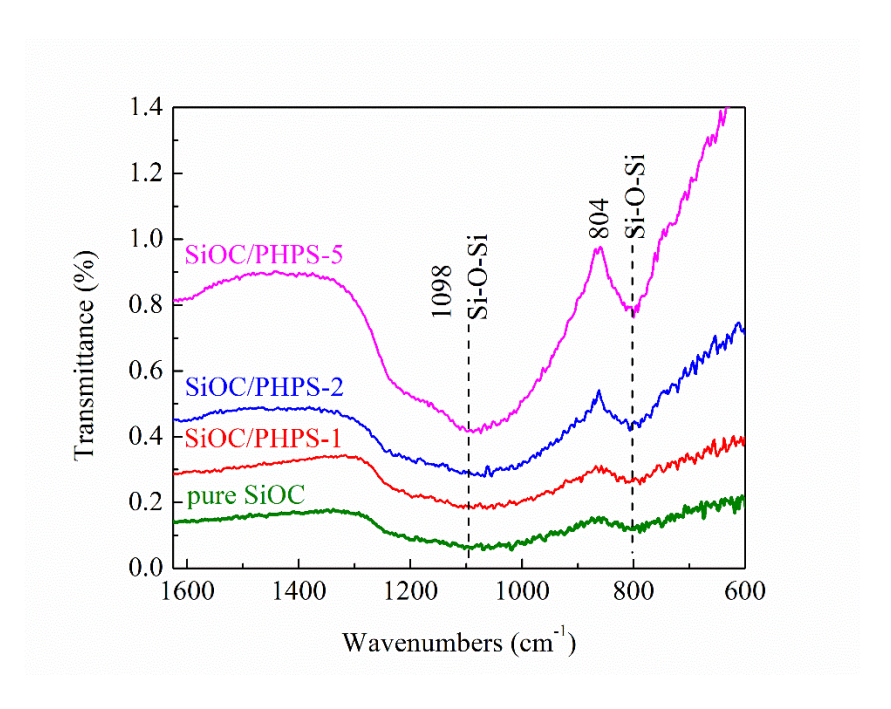
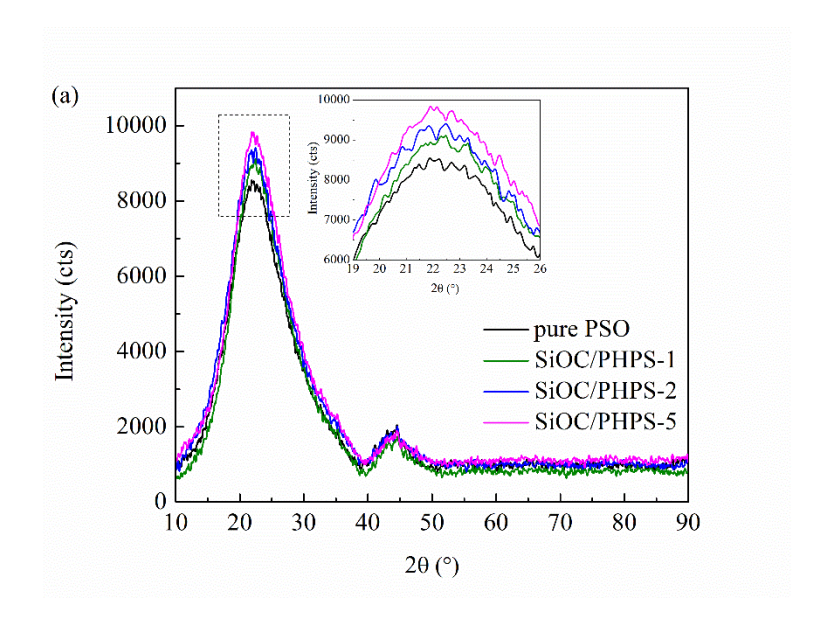
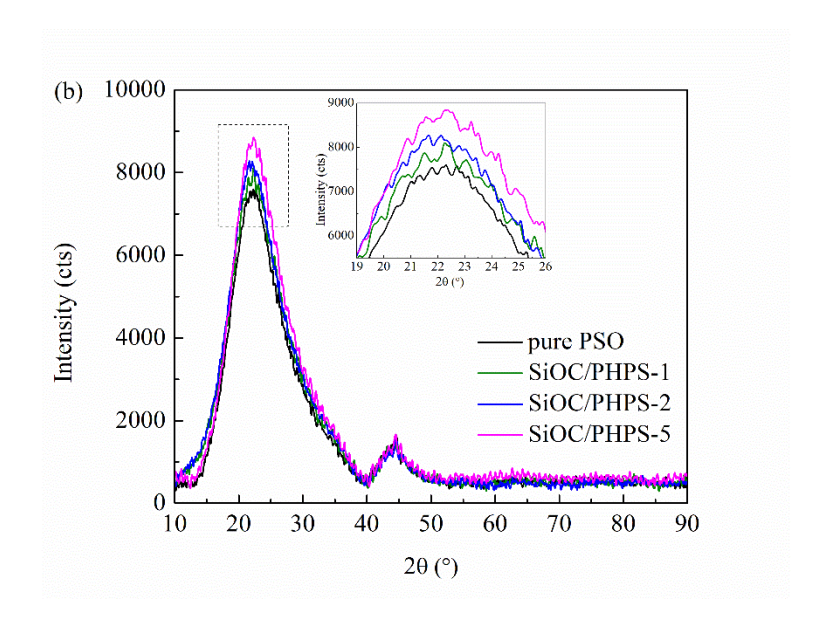


Fig. 3. FTIR spectra of the SiOC samples with different amounts of PHPS at 1200 °C pyrolysis temperature before the HF etching.

The effect of the PHPS addition on the phase evolution is also reflected in the XRD patterns (Fig. 4). All the pyrolyzed samples are amorphous. Only two broad diffraction peaks located at 43° for turbostratic carbon and 23° for amorphous SiO₂ [34] are observed. In the process of sample preparation, the content of PSO is always constant, and the only variable is the content of PHPS. Since there are no C atoms in PHPS, the carbon content in all the samples with different amounts of PHPS should be constant. Thus, the intensity ratio of SiO₂ to turbostratic carbon (I_{silica}/I_{carbon}) (supplement Table S2) can be represented as the level of SiO₂ formation. The value of I_{silica}/I_{carbon} increases with the PHPS addition, at 2.63, 3.03, 3.00, and 3.16 for the pure SiOC, SiOC/PHPS-1, SiOC/PHPS-2, and SiOC/PHPS-5, respectively. This means that the addition of PHPS accelerates the formation of Si-O-Si and nucleation of the SiO₂ nanodomains, consistent with the results in Figs. 3-4. A similar trend is also observed at 1200 and 1300 °C pyrolysis temperatures (Figs. 4(b))

and (c)). All the pyrolyzed samples are amorphous in Fig. 4(c) without additional peaks. Even at higher pyrolysis temperatures, the samples still only show the peaks of turbostratic carbon and amorphous SiO₂. As discussed in Part 3.1, the presence of water vapor during the pyrolysis can significantly affect the subsequent phase separation of the SiOC matrix. Different from the SiOC samples pyrolyzed in pure Ar, the water vapor reacts with free carbon and certain organic species in the preceramics and generates extensive Si-OH groups to form SiO₂ nanodomains. The reduction of Si-C bonds in the matrix suppresses the precipitation of SiC at higher pyrolysis temperatures [24]. This is why there is no significant difference among Figs. 4(a-c). Overall, the formation of SiO₂ is more evident for the samples with higher PHPS additions.





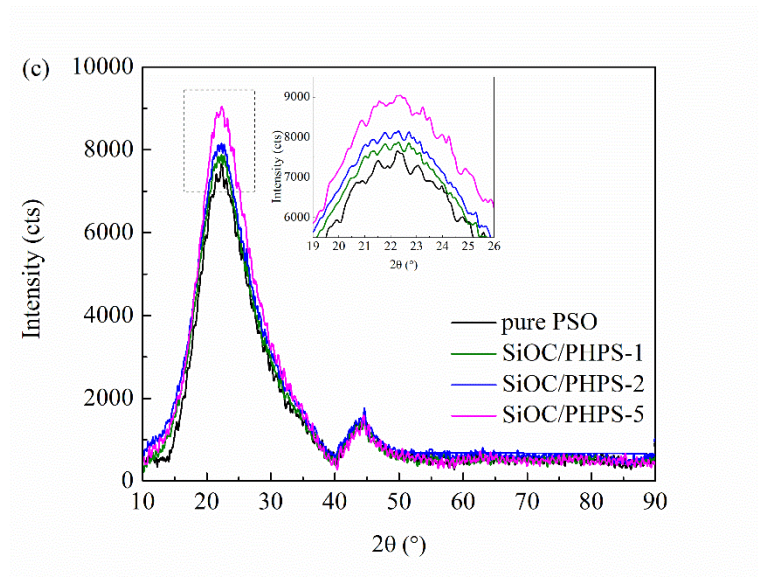


Fig. 4. Amorphous SiO₂ peaks of all the SiOC samples pyrolyzed at (a) 1100 °C, (b) 1200 °C, and (c) 1300 °C.

With more SiO₂ nanodomains dispersed in the SiOC matrix, highly porous microstructures can be obtained by removal of SiO₂ with HF etching:

$$SiO_2 + HF \rightarrow H_2SiF_6 + H_2O \tag{12}$$

Since SiOC is resistant to HF acid, presumably only the SiO₂ nanodomains can be etched way. SiO₂ can act as a pore-forming agent for the SiOC matrix. For the pure SiOC pyrolyzed at 1100 °C, the etching mass loss is 61.9 wt% as displayed in Fig. 5. With an increasing addition of PHPS, the mass loss after etching slightly increases. A similar trend is also observed for the samples pyrolyzed at 1200 and 1300 °C. An addition of PHPS results in a slight increase in the mass loss after etching compared with the pure PSO in Fig. 5 at different pyrolysis temperatures. As a result, it is reasonable to believe that PHPS accelerates the nucleation of the SiO₂ nanodomains in the SiOC matrix. As for the effect of the pyrolysis temperature, the etching mass loss increases from 1100 °C to 1300 °C for all the samples because of more advanced SiOC phase separation.

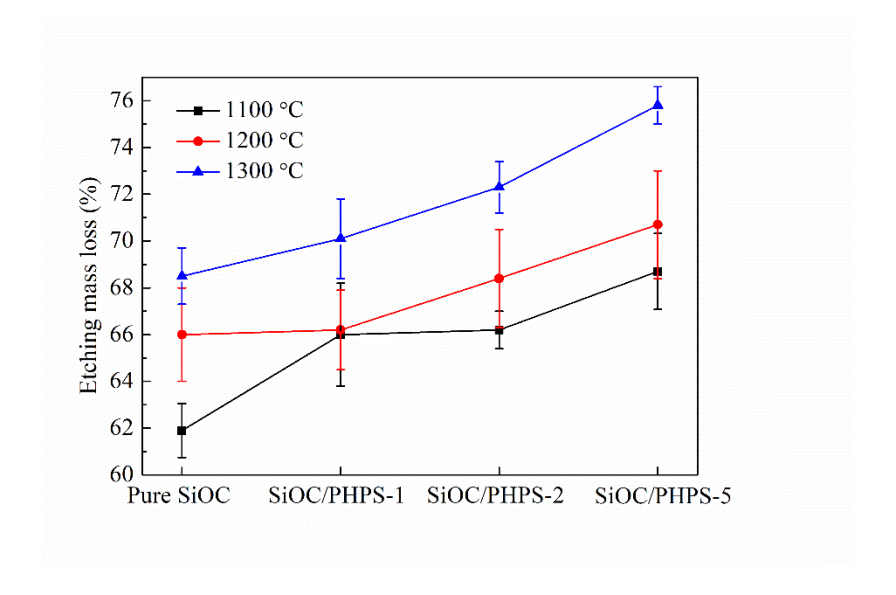
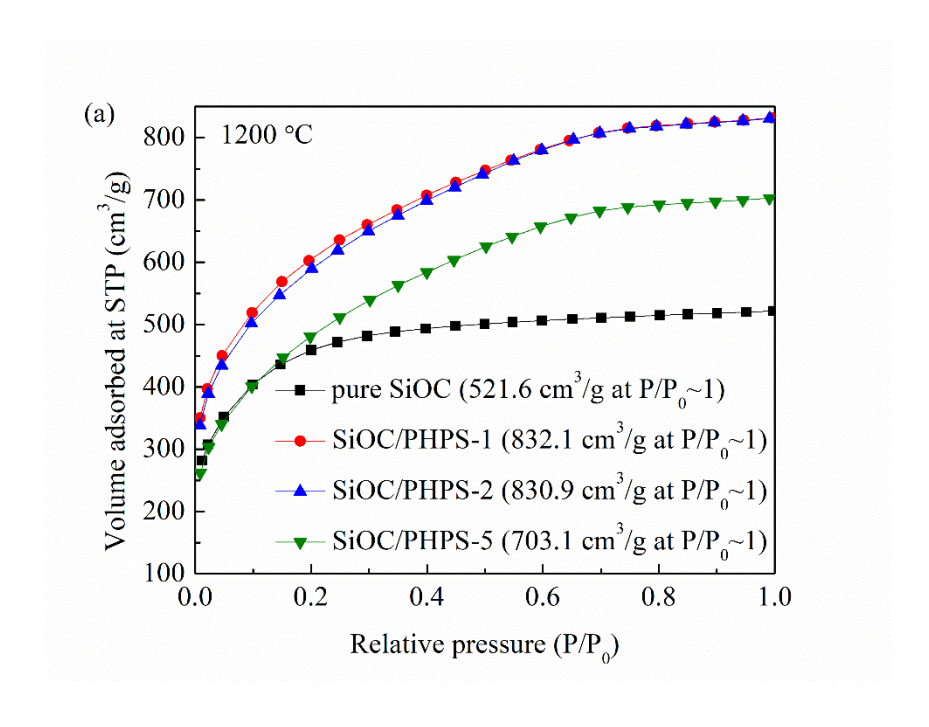


Fig. 5. Etching mass loss of different samples pyrolyzed at 1100, 1200, and 1300 °C.

3. 3. Specific surface area and pore size

Fig. 6(a) shows the adsorption isotherms of all the samples with different PHPS contents pyrolyzed at 1200 °C after the HF etching. For all the samples, the hysteresis loop is very narrow, and the adsorption and desorption curves are almost the same. The inserted pore size distribution

in Fig. 6(b) shows that the nanopores for the pure SiOC are in the range of 1-2 nm, whereas larger pores from ~2.3 nm to 6 nm exist in the SiOC/PHPS samples. For the pure SiOC sample, the N₂ gas adsorption volume is lowest, at 521.6 cm³/g. For the SiOC/PHPS-1, SiOC/PHPS-2, and SiOC/PHPS-5 samples, the gas adsorption volumes are 832.1, 830.9, and 703.1 cm³/g, respectively. The gas adsorption volume decreases with an increasing addition of PHPS. The phase-separated SiO₂ leads to a maximum adsorption volume of 832.1 cm³/g for SiOC/PHPS-1.



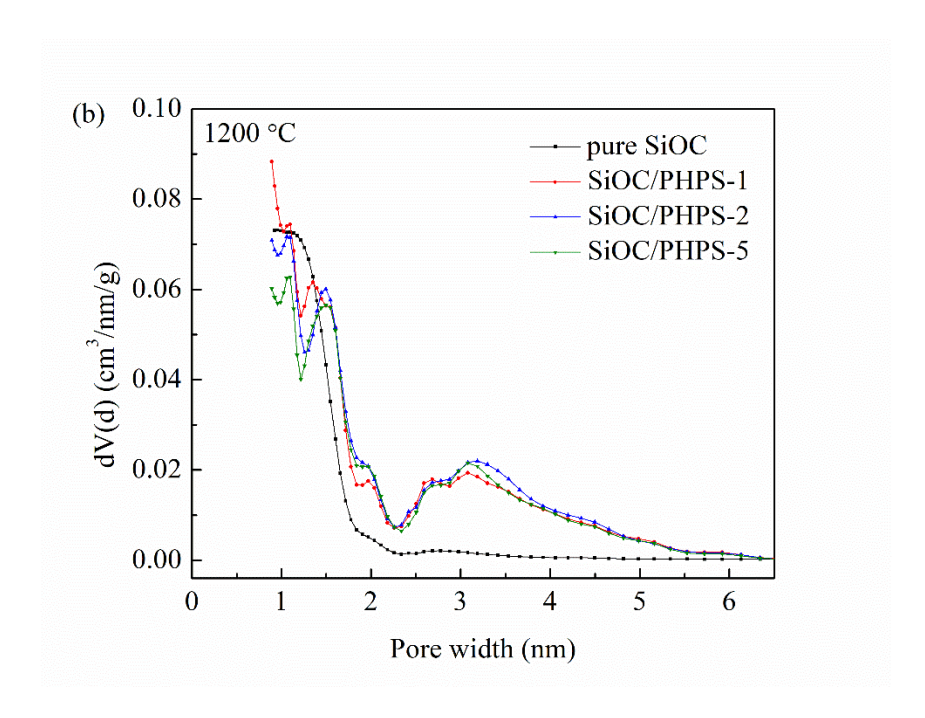


Fig. 6. (a) Nitrogen adsorption-desorption isotherms, (b) pore size distributions of the pure SiOC, SiOC/PHPS-1, SiOC/PHPS-2, and SiOC/PHPS-5 samples pyrolyzed at 1200°C after etching.

The pore size distributions of all the samples pyrolyzed at 1200 °C are displayed in Fig. 6(b). For the SiOC samples, the pore sizes are less than 2 nm without any pores of >2.3 nm size. With the addition of PHPS, the pore size distribution has additional high peaks at 2.3-5 nm, which is not seen for the pure SiOC sample. This indicates that the SiOC ceramics with PHPS additives consist of small (<2 nm) and large (2.3-5 nm) pores. We conjuncture that the small pores are from the SiOC phase-separated SiO₂ domains and the large ones are from the evolution of the PHPS additive. Certain properties of the resulting porous SiOC ceramic such as the morphology and distribution uniformity of pores have been investigated in our previous paper [13], the pores were uniformly distributed and their spherical shapes do not change after high temperature annealing.

The specific surface areas (SSA) of the different temperature pyrolyzed samples after the HF etching are shown in Fig. 7, which are determined by the NLDFT theory [35]. For the pure SiOC samples, the SSA increases from 1211.3 m^2/g (1100 °C) to 1751.3 m^2/g (1300 °C) due to the phaseseparated SiO₂ domains from SiOC at elevated temperatures. In comparison, the SSA of the pure SiOC pyrolyzed at 1300 °C in pure Ar without any water vapor [13] was reported to be ~ 630.4 m²/g by HF etching. The presence of water vapor during pyrolysis indeed accelerates the formation of SiO₂ nanodomains and then results in higher SSA. In addition, the SSA of the pure SiOC increases with the pyrolysis temperature. However, the effect of pyrolysis temperature on the SSA of the PHPS-containing samples is more complicated. For SiOC/PHPS-1, the SSA increases from 1359.7 (1100 °C) to 2079.3 m²/g (1200 °C), before dropping to 1867.6 m²/g at 1300 °C. For SiOC/PHPS-2, the SSA increases from 1622.0 m²/g to 2036.7 m²/g and then decreases to 1806.7 m²/g after 1300 °C pyrolysis. Overall, the SSAs of the SiOC/PHPS-1 and SiOC/PHPS-2 samples increase drastically from 1100 °C to 1200 °C pyrolysis temperature, and subsequently decrease from 1200 °C to 1300 °C. This can be explained based on the understanding that continuous growth of the SiO₂ phase causes larger pore sizes and leads to a decline in the SSA. However, this explanation cannot be fitted to the SiOC/PHPS-5 sample. Different from all the other samples, the SSA of SiOC/PHPS-5 continuously decreases from 2035.6 to 1677.7 m²/g from 1100 to 1300 °C pyrolysis temperature. The above discussion and conclusions also apply to the SSAs derived from the BET model. Specific data values are given in the supplementary Table S3.

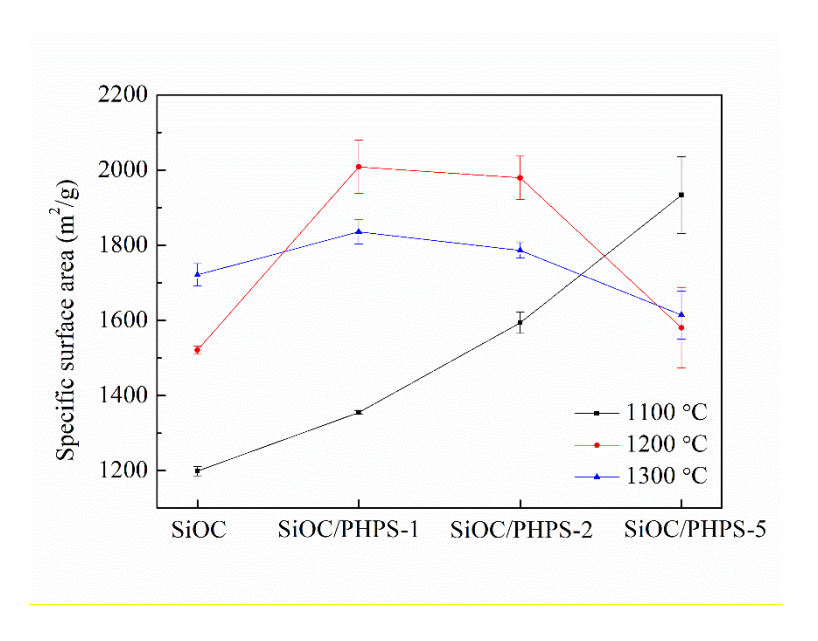


Fig. 7. Specific surface areas of all the samples at different pyrolysis temperatures.

At the same pyrolysis temperature, the change in SSA depends on the amount of the PHPS additive. When the pyrolysis temperature is 1100 °C, the SSA of the samples increases with the additive content. When the additive content is highest (SiOC/PHPS-5), the SSA of the samples reaches a maximum value of 1934.2 m²/g at 1100 °C. At 1200 and 1300 °C, the SSA increases from the pure SiOC to SiOC/PHPS-2, and then decreases from SiOC/PHPS-2 to SiOC/PHPS-5. Again, higher pyrolysis temperature causes further phase separation of the SiOC matrix and prompts more SiO₂ nanodomain formation. If the amount of the SiO₂ phase is excessive (in the high PHPS content sample SiOC/PHPS-5), the aggregation of the SiO₂ phase causes the SSA to decrease. This means that the PHPS additive content and the pyrolysis temperature have a convoluting effect on the SSA, depending on the specific impact on the SiO₂ nanodomain formation.

As Fig. 8 shows, the average pore size increases with the pyrolysis temperature and the PHPS additive amount. At 1100 °C pyrolysis temperature, the average pore size for all the samples is

~1.3 nm. With the temperature increase to 1200 °C and then to 1300 °C, pore growth becomes more obvious, especially for the SiOC/PHPS-5. The average pore size from SiOC/PHPS-5 increases from ~1.7 nm to ~4 nm at 1300 °C. A possible explanation for this drastic increase in pore size for SiOC/PHPS-5 at 1300 °C is the merging of the SiO₂ domains. Both higher PHPS content and higher pyrolysis temperature promote the nucleation and growth of the SiO₂ phase.

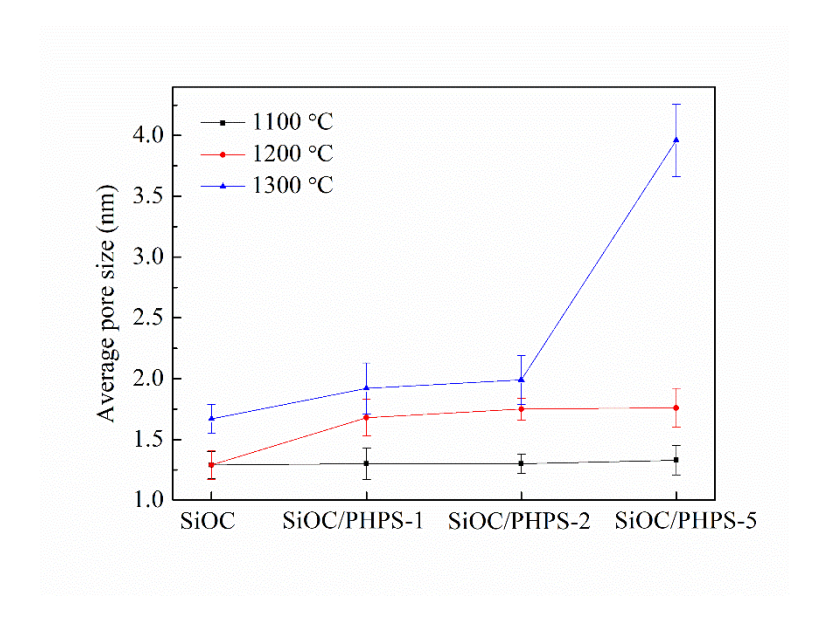


Fig. 8. Average pore size of all the samples at different pyrolysis temperatures.

3. 4. Model understanding

To further understand the effect of SiO₂ nanodomains on the characteristics of the porous SiOC ceramics, a composition-based geometric model based on Saha et al.'s work [36-38] can be applied to the current work. For SiOC systems, the model describes a cellular structure of SiO₂ nanodomains surrounded by graphene layers and mixed bonds of Si-O-C (SiOC₃, SiO₂C₂, and SiO₃C). In other words, a SiOC material can be constructed from three constituents: clusters of SiO₂ tetrahedra that form the centers of the domains, the surrounding SiC_nO_{4-n} layers, where n alters the fourfold coordination of silicon to carbon and oxygen, and the graphene cage-like

network that encases the domains. However, the domain wall thickness derived from this model is based on the assumption that pores have cylindrical shapes. In general, spherical pores remain in the SiOC network after HF etching of the SiO₂ nanodomains [39]. In this section, we will refine this model and estimate the thickness of the above domain walls, which are left as a porous network after etching.

To quantitatively calculate the width of the domain walls, we assume that: (1) HF etching process only removes SiO_2 without the removal of carbon [37], (2) all the SiO_2 phase is removed during etching, (3) the graphene layer and the mixed SiOC tetrahedra exist as "walls" in the etched samples, and (4) all the pores are spherical. In our revised model, d_n is the inner diameter of the spherical pores and equals to the pore size measured from the adsorption isotherms in Fig. 6(b). The average distance between two pores is λ , and then the volume fraction of the pores (V₀) can be expressed as

$$V_0 = \frac{\pi d_n^3}{6\lambda^3} \tag{13}$$

Thus the porous SiOC has a volume fraction of 1-V_o, and the wall volume fraction is:

$$\frac{\pi d_n^2 \delta}{\lambda^3} = 2(1 - V_0) \tag{14}$$

Then the wall thickness (δ) can be calculated according to:

$$\delta = \frac{(1 - V_0)d_n}{3V_0} \tag{15}$$

 δ is related to the measured pore size and pore volume. V_o can be obtained from the density and specific pore volume (Table 2) of the N_2 adsorption measurements.

Table 2. Parameters related to the etched SiOC and SiOC/PHPS samples pyrolyzed at 1200 °C.

| | Etched | Specific pore | Average | Average | Average |
|-------------|----------------------|----------------------|----------|-----------|-----------|
| Sample | density | volume | volume | pore size | wall |
| | (g/cm ³) | (cm ³ /g) | fraction | (nm) | thickness |
| | | | | | (nm) |
| Pure SiOC | 0.55 | 0.75 | 0.41 | 1.29 | 0.62 |
| SiOC/PHPS-1 | 0.52 | 1.34 | 0.70 | 1.68 | 0.24 |
| SiOC/PHPS-2 | 0.53 | 1.21 | 0.64 | 1.75 | 0.33 |
| SiOC/PHPS-5 | 0.54 | 1.02 | 0.55 | 1.76 | 0.48 |

In Table 2, the average wall thickness δ , also the effective width of the interface between SiO₂ domains, varies with the amount of PHPS addition. For the pure SiOC without any additives, δ has a relatively large average value of 0.62 nm. With the increase of the PHPS content, which means V_0 increase, δ decreases. At the low PHPS content (SiOC/PHPS-1), the SiO₂ nanodomains derived from PHPS are small enough to co-exist with the SiO₂ nanoclusters from the PSO-based SiOC phase separation. This in turn should produce a high SSA after the HF etching, which is also confirmed in Fig. 7. Compared to the pure SiOC, SiOC/PHPS-2, and SiOC/PHPS-5 samples, the average δ value of the SiOC/PHPS-1 sample is lowest at 0.26 nm. Theoretically, the thickness of a single-layer graphene is 0.345 nm. This means that the average wall between the SiO₂ domains for SiOC/PHPS-1 consists of only silicon mixed bonds without any graphene layer. Our previous study [23] also shows that the value of SSA decreases with an increase of graphene layers, consistent with the value of SiOC/PHPS-2 (0.33 nm) and SiOC/PHPS-5 samples (0.48 nm) in this study.

Except for the average wall thickness, the distribution of the wall thicknesses between the SiO₂ domains at 1200 °C pyrolysis temperature can be calculated and displayed in Fig. 9. The wall thickness of the pure SiOC at 1200 °C is the largest. With more addition of PHPS, the wall thickness distribution curve moves towards smaller values. Overall, the PHPS addition leads to pore wall thickness decrease. In order to explain this phenomenon, Fig. 10 displays the relation between the SiO₂ size and the domain wall thickness. Without any addition of PHPS in Fig. 10(a), a thicker graphene layer and a few SiC_nO_{4-n} tetrahedra separate the SiO₂ clusters. Because of the limited number of the SiO₂ sites, the thickness of the domain wall (the layer between the green circle and the black square) is relatively large. Since the PHPS additive creates more Si-O-Si bonds during the pyrolysis, the graphene layers and SiC_nO_{4-n} tetrahedra have to be shared among more SiO₂ sites, which results in a thinner domain wall in Fig. 10(b). Based on equation (13), the wall thickness not only depends on the pore size, but also on the pore volume fraction. When comparing different SiOC/PHPS samples, the wall thickness increases with more PHPS. We believe it is caused by the decrease of the SiO₂ sites due to the merging effect even though the total number of the SiO₂ sites is still much more than that of the pure SiOC.

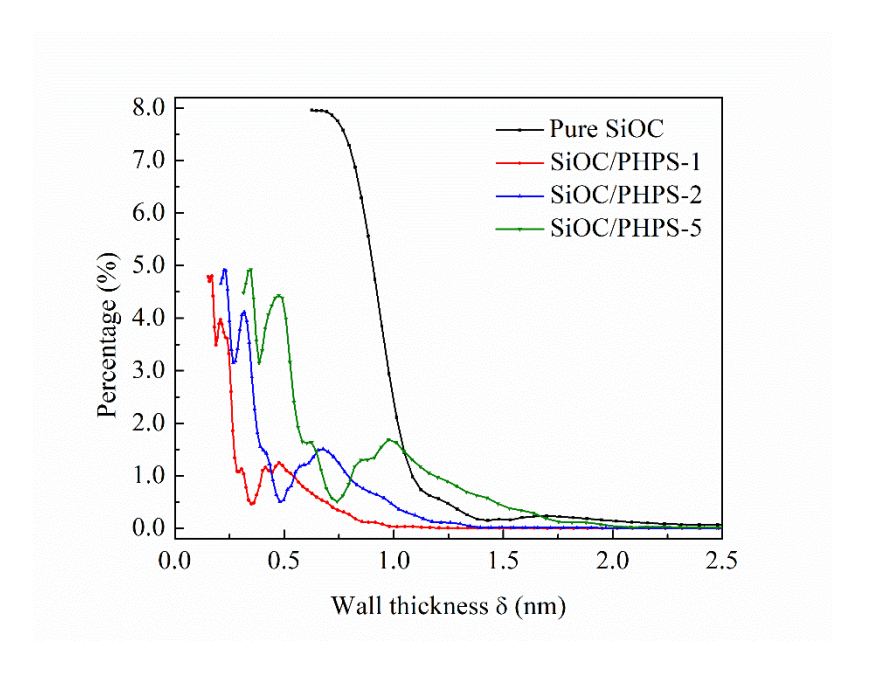


Fig. 9. Distribution of domain wall thicknesses for all the SiOC samples pyrolyzed at 1200 °C after the HF etching.

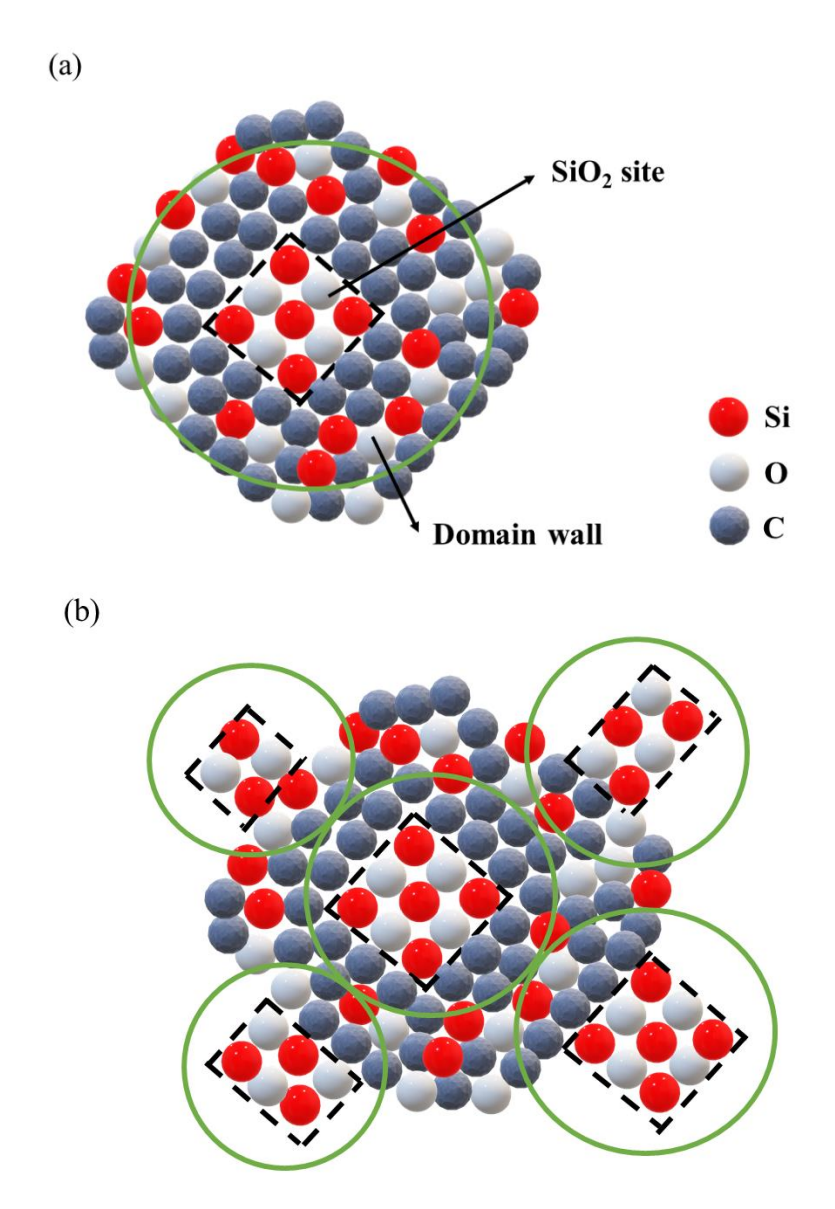


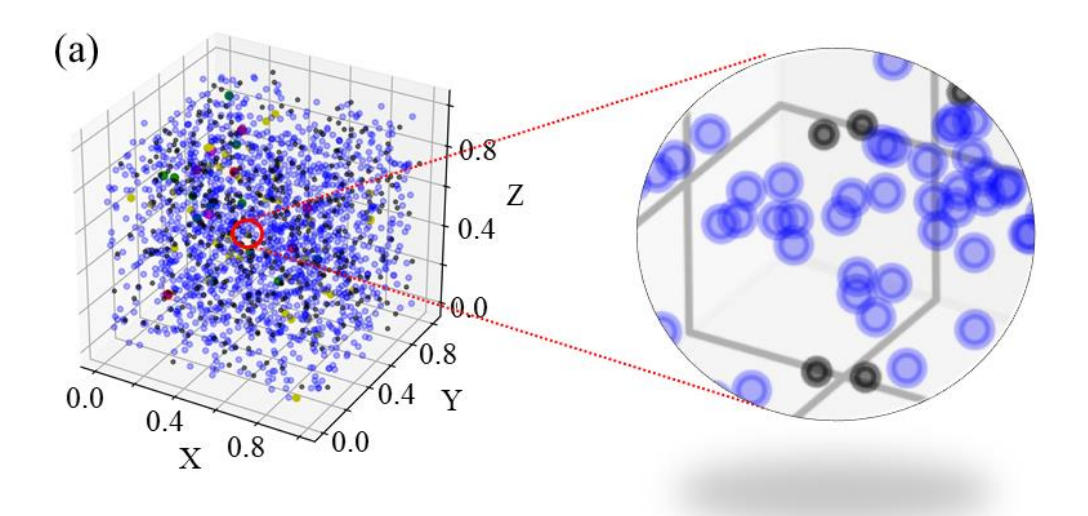
Fig. 10. Illustration of the etched SiOC matrix without PHPS additive (a) and with PHPS additive.

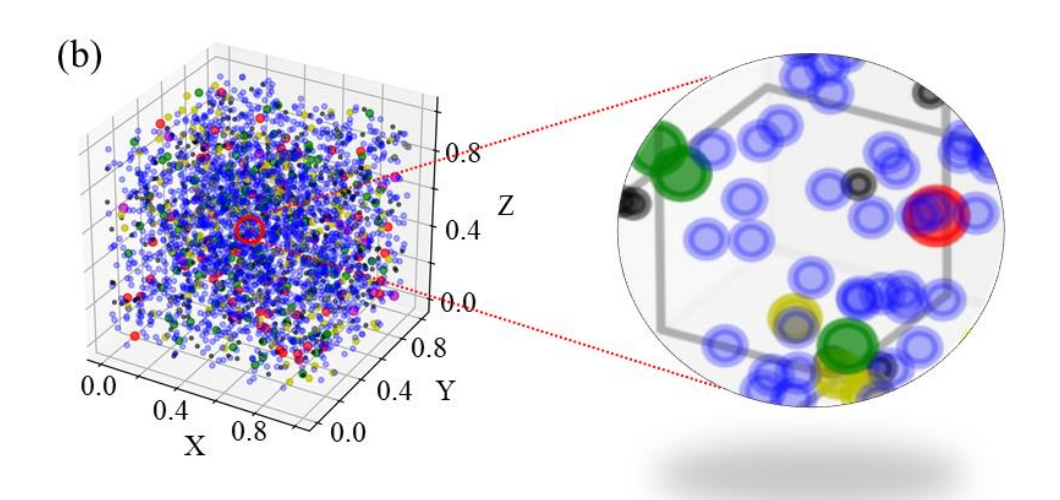
3D views of SiO₂ domain distributions can further explain the effect of PHPS addition on the wall thickness and SSA of the etched SiOCs. Fig. 11 shows 3D plots of randomly distributed SiO₂ domains in the pyrolyzed samples at 1200 °C. The side length of each cuboid unit is expressed as

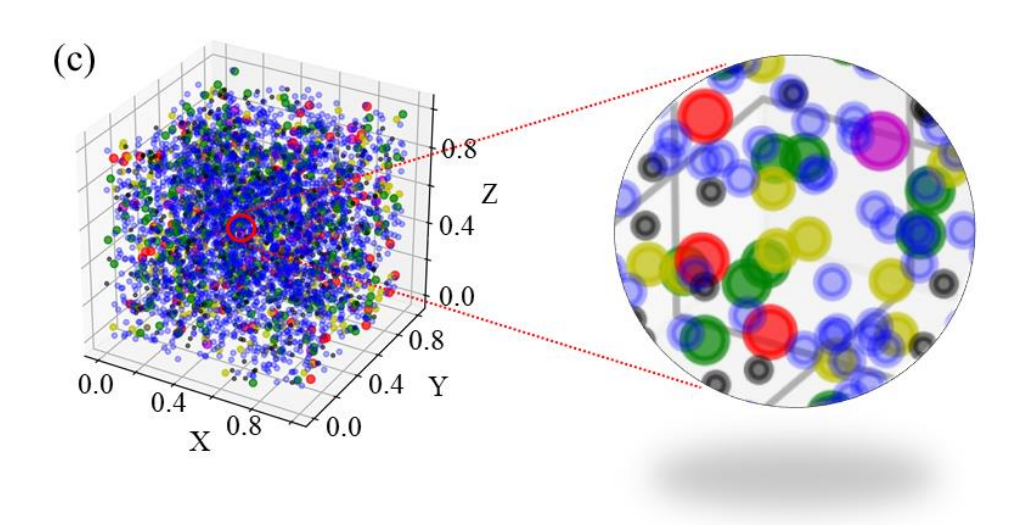
1 and the number of SiO_2 domains n_{SiO_2} in the cuboid can be calculated based on the following equation:

$$n_{SiO_2} = \frac{\rho_b V_p \alpha}{V_{SiO_2}} \tag{16}$$

where ρ_b is the bulk density of the etched sample, V_{SiO_2} is the average volume for each SiO₂ tetrahedron obtained from the average pore size. α is the mole ratio of Si atoms in the PHPS:PSO precursors. V_p is the specific pore volume (cm³/g). With more PHPS addition, n_{SiO_2} increases. Based on the simulation results from the 3D random function in Python, the SiO₂ nanodomains from the phase separation of the pure SiOC are uniformly dispersed without any aggregation, as shown in Fig. 11(a). Based on Fig. 6(b), pores larger than 2.3 nm are not evident. With an increasing amount of the PHPS additive, more SiO₂ nanoclusters are formed, along with larger sizes. The 3D simulation results show that small pores, in the range of 1-2 nm, are more likely to aggregate because of their dominance. This phenomenon is more obvious in Fig. 11(d), which results in more connected pores to decrease the SSA. The plots in Fig. 11 also explain the results in Fig. 10. More SiO₂ nanoclusters are formed to decrease the wall thickness by sharing the graphene and SiC_nO_{4-n} tetrahedra. A thin wall results in a higher SSA value; However, the merging effect of the nanopores is more dominant in decreasing SSA. It should be mentioned that the amorphous nature of the SiOC species and the similar atomic number to amorphous SiO₂ make any attempt to distinguish these phases using imaging almost impossible. Currently, we are carrying out high-speed 4D STEM diffraction analysis in order to understand the multiple phase distributions of SiOC. Hopefully, it will shed additional light on the SiO2 nanodomains and their distributions.







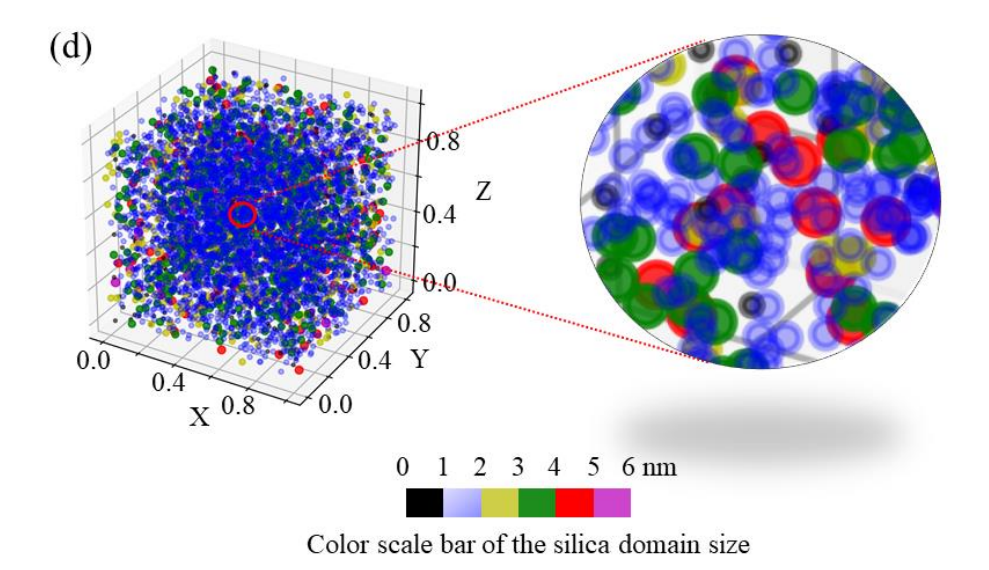


Fig. 11. 3D pore distributions of (a) pure SiOC, (b) SiOC/PHPS-1, (c) SiOC/PHPS-2, and (d) SiOC/PHPS-5 samples after 1200 °C pyrolysis and HF etching.

Fig. 12 plots the SSA and reciprocal of the average wall thickness for all the samples pyrolyzed at 1200 °C. The change for the SSA is similar to that of the reciprocal of the average wall thickness. It proves that a thicker wall result in a lower SSA. It is worth mentioning that the specific pore volume of the pure SiOC, SiOC/PHPS-1, SiOC/PHPS-2, and SiOC/PHPS-5 are 0.75, 1.34, 1.21, and 1.02 cm³/g respectively, as listed in Table 2. In general, the specific pore volume should increase with the addition of PHPS (SiO₂ fillers). However, the experimental data only reach a maximum (1.34 cm³/g) for SiOC/PHPS-1 before decreasing to the lowest value for SiOC/PHPS-5. In Fig. 9, the overall value of the wall thickness moves towards higher values, from SiOC/PHPS-1 to SiOC/PHPS-5. A higher wall thickness likely prevents the removal of the SiO₂ domains by the HF etching, resulting in lower values of specific pore volume and SSA with higher addition of PHPS. In order to create an ultrahigh SSA, small and separated SiO₂ nanoclusters with thin walls are necessary.

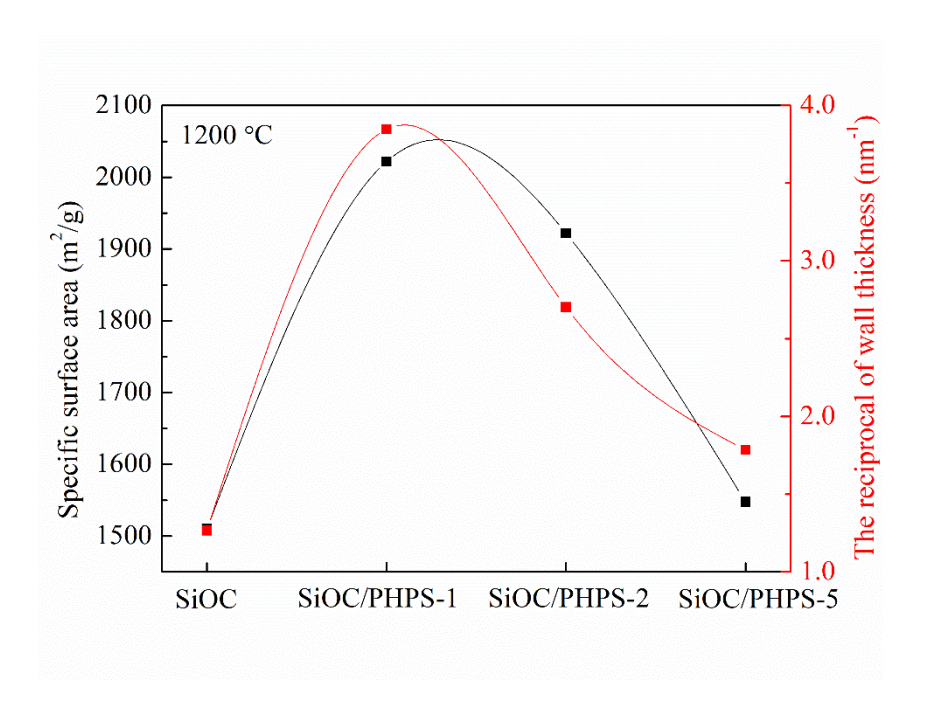


Fig. 12. Comparison between the SSA and reciprocal of wall thickness for the SiOC samples pyrolyzed at 1200 °C.

4. Conclusions

This paper reports on creation of ultrahigh surface area SiOC ceramics based on PHPS and PSO. PHPS hydrolysis and chemical anchoring to PSO by crosslinking lead to more Si–O-Si bonds after pyrolysis. The resulting SiO₂ nanodomains can be etched to create ~2 nm size pores. The specific surface area of the SiOC/PHPS samples is up to ~2000 m²/g. The SiO₂ nanodomain impact on the specific surface area and pore size is studied based on the calculation of wall thickness for graphene layers and mixed Si-O-C bonds. 3D view of SiO₂ domains can further explain the microstructural evolution. Small and separated SiO₂ nanoclusters with thin domain walls are critical in creating ultrahigh SSA. Such high surface area and micro-/meso-porous materials should have important applications in catalysis, gas separation, molecular sieves, among others.

Acknowledgment:

We acknowledge the financial support from National Science Foundation under grant number CMMI-1634325.

References:

- [1] P.S. Liu, G.F. Chen (Eds.), Porous Materials, Butterworth-Heinemann, Boston, 2014, pp. 1-20.
- [2] V.R. Salvini, V.C. Pandolfelli, D. Spinelli, Recent Adv. Porous Ceram. (2018) 171, http://dx.doi.org/10.5772/intechopen.71612.
- [3] H. Bréquel, J. Parmentier, S. Walter, R. Badheka, G. Trimmel, S. Masse, J. Latournerie, P. Dempsey, C. Turquat, A. Desmartin-Chomel, Chem. Mater. 16 (2004) 2585-2598, https://doi.org/10.1021/cm049847a.
- [4] N. Yang, M. Gao, L. Jiefang, K. Lu, J. Am. Ceram. Soc. 1 (2020) 145-157, https://doi.org/10.1111/jace.16738.
- [5] D. Erb, K. Lu, Mater. Chem. Phys. 237 (2019) 121844, https://doi.org/10.1111/j.1551-2916.2010.03876.x.
- [6] N. Yang, K. Lu, J. Eur. Ceram. Soc. 39 (2019) 4029-4037, https://doi.org/10.1016/j.jeurceramsoc.2019.06.020.
- [7] K. Lu, D. Erb, M. Liu, J. Mater. Chem. C 4 (2016) 1829-1837, https://doi.org/10.1039/C6TC00069J.
- [8] T. Xu, Q. Ma, Z. Chen, High-temperature behavior of silicon oxycarbide glasses in air environment, Ceram Int. 37 (2011) 2555-2559, https://doi.org/10.1016/j.ceramint.2011.03.053.
- [9] C.G. Pantano, A.K. Singh, H. Zhang, J. Sol-Gel Sci. Technol. 14 (1999) 7-25, https://doi.org/10.1023/A:1008765829012.
- [10] B. Du, C. Hong, A. Wang, S. Zhou, Q. Qu, S. Zhou, X. Zhang, Ceram Int. 44 (2018) 563-570, https://doi.org/10.1016/j.ceramint.2017.09.212.
- [11] J. Qian, X. Wang, C. He, M. Cai, P. Hu, A. Shui, B. Du, Ceram Int. 45 (2019) 24331-24335, https://doi.org/10.1016/j.ceramint.2019.08.148.

- [12] K. Lu, D. Erb, K. Bawane, N. Yang, J. Eur. Ceram. Soc. 39 (2019) 3035-3041, https://doi.org/10.1016/j.jeurceramsoc.2019.03.051.
- [13] J. Li, K. Lu, T. Lin, F. Shen, J. Am. Ceram. Soc. 98 (2015) 1753-1761, https://doi.org/10.1111/jace.13541.
- [14] J. Li, K. Lu, J. Am. Ceram. Soc. 98 (2015) 2357-2365, https://doi.org/10.1111/jace.13634.
- [15] M. Naviroj, S. Miller, P. Colombo, K. Faber, J. Eur. Ceram. Soc. 35 (2015) 2225-2232, https://doi.org/10.1016/j.jeurceramsoc.2015.02.013.
- [16] B.M. Kumar, Y.-W. Kim, Sci. Technol. Adv. Mater. 11 (2010) 044303, https://doi.org/10.1088/1468-6996/11/4/044303.
- [17] C. Vakifahmetoglu, P. Colombo, Adv. Eng. Mater. 10 (2008) 256-259, https://doi.org/10.1002/adem.200700330.
- [18] J. Wu, Y. Li, L. Chen, Z. Zhang, D. Wang, C. Xu, J. Mater. Chem. 22 (2012) 6542-6545, https://doi.org/10.1039/C2JM16840E.
- [19] R. Ahmad, J.-H. Ha, I.-H. Song, J. Korean Powder Metall. Inst. 21 (2014) 389-398, https://doi.org/10.4150/KPMI.2014.21.5.389.
- [20] P. Colombo, J. Eur. Ceram. Soc. 28 (2008) 1389-1395, https://doi.org/10.1016/j.jeurceramsoc.2007.12.002.
- [21] D. Erb, K. Lu, J. Eur. Ceram. Soc. 37 (2017) 4547-4557, https://doi.org/10.1016/j.jeurceramsoc.2017.06.036.
- [22] D. Erb, K. Lu, Mater. Chem. Phys. 209 (2018) 217-226, https://doi.org/10.1016/j.matchemphys.2018.01.078.
- [23] D. Erb, K. Lu, Microporous Mesoporous Mater. 266 (2018) 75-82, https://doi.org/10.1016/j.micromeso.2018.02.034.
- [24] K. Lu, J. Li, J. Eur. Ceram. Soc. 36 (2016) 411-422, https://doi.org/10.1016/j.jeurceramsoc.2015.11.003.
- [25] A. Morlier, S. Cros, J.-P. Garandet, N. Alberola, Thin Solid Films 524 (2012) 62-66, https://doi.org/10.1016/j.tsf.2012.09.065.
- [26] L. Prager, A. Dierdorf, H. Liebe, S. Naumov, S. Stojanović, R. Heller, L. Wennrich, M.R. Buchmeiser, Chem: Eur. J. 13 (2007) 8522-8529, https://doi.org/10.1002/chem.200700351.
- [27] A. Lavedrine, D. Bahloul, P. Goursat, N.C.K. Yive, R. Corriu, D. Leclerq, H. Mutin, A. Vioux, J. Eur. Ceram. Soc. 8 (1991) 221-227, https://doi.org/10.1016/0955-2219(91)90098-K.

- [28] C.J. Liu, S.-S. Lin, Y. Zheng, S.-Y. Chen, P. Shen, Cryst. Eng. Comm. 17 (2015) 9142-9154, https://doi.org/10.1039/C5CE01752A.
- [29] N.P. Bansal, A.R. Boccaccini, Ceramics and composites processing methods, John Wiley & Sons, 2012.
- [30] Z. Zhang, Z. Shao, Y. Luo, P. An, M. Zhang, C. Xu, Polym. Int. 64 (2015) 971-978, https://doi.org/10.1002/pi.4871.
- [31] J.D. Torrey, R.K. Bordia, J. Mater. Res. 22 (2007) 1959-1966, https://doi.org/10.4028/www.scientific.net/MSF.825-826.645.
- [32] K. Wang, X. Zheng, F.S. Ohuchi, R.K. Bordia, J. Am. Ceram. Soc. 95 (2012) 3722-3725, https://doi.org/10.1111/jace.12045.
- [33] J.V.G. Tinio, K.T. Simfroso, A.D.M.V. Peguit, R.T. Candidato, J. Nanotechnol. 2015 (2015), https://doi.org/10.1155/2015/686021.
- [34] D. Erb, K. Lu, J. Am. Ceram. Soc. 101 (2018) 5378-5388, https://doi.org/10.1111/jace.15876.
- [35] G. Kupgan, T.P. Liyana-Arachchi, C.M. Colina, Langmuir 33 (2017) 11138-11145, https://doi.org/10.1021/acs.langmuir.7b01961.
- [36] A. Saha, R. Raj, D. Williamson, H.J. Kleebe, J. Am. Ceram. Soc. 88 (2005) 232-234, https://doi.org/10.1111/j.1551-2916.2004.00034.x.
- [37] R. Peña- Alonso, G.D. Sorarù, R. Raj, J. Am. Ceram. Soc. 89 (2006) 2473-2480, https://doi.org/10.1111/j.1551-2916.2006.01117.x.
- [38] A. Saha, R. Raj, D.L. Williamson, J. Am. Ceram. Soc, 89 (2006) 2188-2195, https://doi.org/10.1111/j.1551-2916.2006.00920.x.
- [39] S. Dire, V. Tagliazucca, L. Salvadori, G.D. Soraru, J. Am. Ceram. Soc, 94 (2011) 3819-3824, https://doi.org/10.1111/j.1551-2916.2011.04732.x.

Supplementary Material

Click here to access/download **Supplementary Material**supplement 04292020.docx

Credit Author Statement

- Ni Yang: Conceptualization; Experimental tasks, Data curation; Formal analysis;
 Investigation; Methodology; Validation; Visualization; Roles/Writing original draft;
 Writing review & editing.
- Kathy Lu: Conceptualization; Formal analysis; Funding acquisition; Investigation;
 Methodology; Project administration; Resources; Software; Supervision; Validation;
 Roles/Writing original draft; Writing review & editing.

Declaration of Interest Statement

Declaration of interests

| oxtimes The authors declare that they have no known competing financial interests or personal relationships that could have appeared to influence the work reported in this paper. | |
|--|---|
| □The authors declare the following financial interests/personal relationships which may be considered as potential competing interests: | |
| | _ |
| | |